High Power Laser Science and Engineering, (2025), Vol. 13, e8, 7 pages.
doi:10.1017/hpl.2024.93

HIGH POWER LASER SCIENCE AND ENGINEERING

RESEARCH ARTICLE

Temporal characterization of ultrashort pulses via reflected four-wave mixing with perturbation on a solid surface

Jinhui Li[1,2,3], Keyang Liu[1,2], Hao Yuan[1,2,3], Xingguo Wang[1,2], Qiwen Zhen[1,2,3], Xianglin Wang[1,2], Yishan Wang[1,2,3], Wei Zhao[1,2,3], Huabao Cao[1,2,3], and Yuxi Fu[1,2,3]

[1] *Center for Attosecond Science and Technology, Xi'an Institute of Optics and Precision Mechanics, Chinese Academy of Sciences, Xi'an, China*

[2] *State Key Laboratory of Ultrafast Optical Science and Technology, Xi'an Institute of Optics and Precision Mechanics, Chinese Academy of Sciences, Xi'an, China*

[3] *University of Chinese Academy of Sciences, Beijing, China*

(Received 27 September 2024; revised 19 November 2024; accepted 13 December 2024)

Abstract

Time-domain characterization of ultrashort pulses is essential for studying interactions between light and matter. Here, we propose and demonstrate an all-optical pulse sampling technique based on reflected four-wave mixing with perturbation on a solid surface. In this method, a weak perturbation pulse perturbs the four-wave mixing signal generated by a strong fundamental pulse. The modulation signal of the four-wave mixing, which is detected in the reflection geometry to ensure a perfect phase-matching condition, directly reflects the temporal profile of the perturbation pulse. We successfully characterized multi-cycle and few-cycle pulses using this method. The reliability of our approach was verified by comparing it to the widely employed frequency-resolved optical gating method. This technique provides a simple and robust method for characterizing ultrashort laser pulses.

Keywords: four-wave mixing; pulse sampling technique; solid surface

1. Introduction

Laser pulses with ultrashort duration are crucial tools for various research fields, including ultrafast spectroscopy[1], attosecond science[2–4], nonlinear frequency conversion[5–7], THz generation[8,9], laser–plasma acceleration[10,11], etc. Accurate temporal characterization of the ultrashort pulse is indispensable for carrying out such applications. Currently, pulse characterization techniques, such as frequency-resolved optical gating (FROG)[12] and D-scan[13], which are indirect reconstruction methods, are widely employed for characterizing the pulses based on various nonlinear processes with simple configurations. Alternatively, direct pulse sampling in the time domain with sub-cycle gates formed by tunnel ionization, multiphoton absorption, high-order harmonic generation, etc., allows for the direct capture of the waveforms of the optical pulses. Techniques like the attosecond streak camera[14], petahertz optical oscilloscope[15], nonlinear photoconductive sampling[16] and tunneling ionization with a perturbation for the time-domain observation of an electric field (TIPTOE)[17,18] have been successfully used for pulse measurement. However, these approaches require either a complex vacuum system or sophisticated photocurrent measuring devices.

Recently, two novel all-optical pulse sampling techniques have been proposed and successfully demonstrated. These techniques involve the introduction of a perturbation to modulate third-order nonlinear processes, specifically transient grating (TG) in solid plates[19] and third-harmonic generation (THG) in ambient air[20]. In these approaches, a weak perturbation pulse modulates the output signal of the third-order nonlinear processes initially generated by a strong fundamental pulse. The output modulation signal of these nonlinear processes directly reflects the temporal profile of the perturbation pulse. These methods have been verified

Correspondence to: K. Liu, H. Cao, and Y. Fu, Center for Attosecond Science and Technology, Xi'an Institute of Optics and Precision Mechanics, Chinese Academy of Sciences, Xi'an 710119, China. Emails: liukeyang@opt.ac.cn (K. Liu); caohuabao@opt.ac.cn (H. Cao); fuyuxi@opt.ac.cn (Y. Fu)

by measuring few-cycle pulses across the near-infrared to mid-infrared range. However, the generation of perturbation and fundamental pulses for these two methods is based on the Mach–Zehnder interferometer, which requires careful alignment. In addition, because the pulses need to pass through several media, which introduce dispersion to the pulses, correction is needed to obtain the spectral phase of the pulses before the measurement setup.

In this study, we present a novel all-optical sampling method for characterizing ultrashort pulses in the temporal domain, which employs reflected four-wave mixing (RFWM) with perturbation on the solid surface. Because the RFWM occurs only at the interface between the air and solid plate, this method can characterize ultra-broadband pulses. In addition, the generation of perturbation and fundamental pulses for this method is realized by division of the wavefront of the input pulse. Thus, the experimental setup is compact, and no correction of the spectral phase is required.

2. Theoretical analysis

When an optical pulse is incident on a solid plate, third-order nonlinear processes such as THG and four-wave mixing occur at sufficiently high pulse intensity. The third-order nonlinear signals can be detected in both transmission and reflection geometries. By employing a weaker pulse to perturb the third-order nonlinear process, the measured signal can be calculated by the following[21]:

$$\begin{aligned} S(\tau) &\propto \int \left[E_{\mathrm{f}}(t)+E_{\mathrm{p}}(t-\tau)\right]^6 \mathrm{d}t \\ &= \int E_{\mathrm{f}}^6(t)\mathrm{d}t + \int 6E_{\mathrm{f}}^5(t)E_{\mathrm{p}}(t-\tau)\,\mathrm{d}t + \\ &\quad \int 15E_{\mathrm{f}}^4(t)E_{\mathrm{p}}^2(t-\tau)\,\mathrm{d}t + \cdots, \end{aligned} \tag{1}$$

where $E_{\mathrm{f}}(t)$ and $E_{\mathrm{p}}(t)$ are the fundamental and perturbation pulses, respectively, and τ is the relative delay between the two pulses. Here, $E_{\mathrm{p}}(t)$ has the same spectrum as $E_{\mathrm{f}}(t)$, but with substantially lower intensity. Thus, the first term on the right-hand side of Equation (1) is constant, and the other terms except the second term are negligible. Then the modulation signal caused by the weak perturbation pulse can be written as follows:

$$\delta(\tau) \propto 6\int E_{\mathrm{f}}^5(t)E_{\mathrm{p}}(t-\tau)\,\mathrm{d}t. \tag{2}$$

It has been demonstrated that $E_{\mathrm{f}}^5(t)$ can be employed as an ultrafast temporal gate to sample $E_{\mathrm{p}}(t)$ when $E_{\mathrm{f}}(t)$ is nearly chirp-free[19,20]. To analyze the influence of the dispersion of $E_{\mathrm{f}}(t)$ on the measurement, Equation (2) is Fourier transformed as follows:

$$\delta(\omega) \propto \mathcal{F}\left[E_{\mathrm{f}}^5(t)\right]^* E_{\mathrm{p}}(\omega), \tag{3}$$

where $\delta(\omega)$ and $E_{\mathrm{p}}(\omega)$ are the spectra of $\delta(\tau)$ and $E_{\mathrm{p}}(t)$, respectively, and $\mathcal{F}\left[E_{\mathrm{f}}^5(t)\right]$ is the Fourier transform of $E_{\mathrm{f}}^5(t)$. Because of the finite bandwidth of $E_{\mathrm{f}}^5(t)$, the bandwidth of $\delta(\omega)$ is slightly narrower than $E_{\mathrm{p}}(\omega)$. Meanwhile, the spectral phase of $E_{\mathrm{f}}^5(t)$ can also introduce error to the retrieved spectral phase of $E_{\mathrm{p}}(\omega)$ if $E_{\mathrm{f}}(t)$ is chirped. Thus, there is discrepancy between $\delta(\omega)$ and $E_{\mathrm{p}}(\omega)$. Nevertheless, the narrowing of the bandwidth can be partially corrected in a simple way. We can assume $E_{\mathrm{f}}(t)$ is chirp-free and the spectrum shape of $E_{\mathrm{f}}(t)$ is identical to $\delta(\tau)$. Thus, $\mathcal{F}\left[E_{\mathrm{f}}^5(t)\right]$ can be easily calculated and then $E_{\mathrm{p}}(\omega)$is approximated by the following:

$$E_{\mathrm{p}}(\omega) \approx \frac{\delta(\omega)}{\mathcal{F}\left[E_{\mathrm{f}}^5(t)\right]^*}. \tag{4}$$

Figure 1(a) shows the influence of group delay dispersion (GDD) on $E_{\mathrm{f}}^5(t)$. The femtosecond pulses centered at 800 nm are taken as an example. The transform limited (TL) pulse duration is 25 fs, which is typical for Ti:sapphire laser pulses[22]. Compared to $E_{\mathrm{f}}(t)$, the spectra of $E_{\mathrm{f}}^5(t)$ are wider and the spectral phases of $E_{\mathrm{f}}^5(t)$ are flatter. With a larger GDD, the bandwidth of $E_{\mathrm{f}}^5(t)$ is smaller, and the dispersion of $E_{\mathrm{f}}^5(t)$ is larger, which is not preferrable for the measurement. The measured pulse durations of 25 fs pulse with different GDDs for $E_{\mathrm{f}}(t)$ are shown in Figure 1(b). It is obvious that the error of the measurement is larger with more chirped $E_{\mathrm{f}}(t)$ if the bandwidth of $E_{\mathrm{p}}(t)$ is not corrected. After correction of the spectra, the measurement error is clearly mitigated, and the error is less than 1 fs (4% of the original pulse duration) when the absolute value of GDD for $E_{\mathrm{p}}(t)$ is not more than 200 fs^2. Here, $E_{\mathrm{p}}(t)$ is stretched to approximately 33 fs with GDD of 200 fs^2, which is about 1.32 times the TL pulse duration. To ensure accurate measurement in the experiment presented here, we tuned the fundamental pulse to near chirp-free by observing the filamentation in the air after tight focusing.

In this work, we choose to measure the modulation signal of the four-wave mixing on a solid surface in the reflection geometry for temporally sampling the ultrashort pulses. The phase-matching is ensured in the reflection geometry, which allows one to characterize pulses with broad bandwidth. The RFWM signal from the surface can be simply expressed as follows:

$$\begin{aligned} P_{\mathrm{RFWM}}(t,\tau) \propto\ & |E_{\mathrm{f}}(t)|^2 E_{\mathrm{f}}(t) + 3|E_{\mathrm{f}}(t)|^2 E_{\mathrm{p}}(t-\tau) + \\ & 3E_{\mathrm{f}}^2(t)\,E_{\mathrm{p}}{}^*(t-\tau) + 3E_{\mathrm{f}}(t)\left|E_{\mathrm{p}}(t-\tau)\right|^2 + \\ & 3E_{\mathrm{f}}(t)^* E_{\mathrm{p}}^2(t-\tau) + \left|E_{\mathrm{p}}(t-\tau)\right|^2 E_{\mathrm{p}}(t-\tau). \end{aligned} \tag{5}$$

The first three terms are detected to obtain the modulation signal of the four-wave mixing, while the last three terms are negligible. The first three terms are non-collinear according to the phase-matching condition (Figure 2(a)). Because the

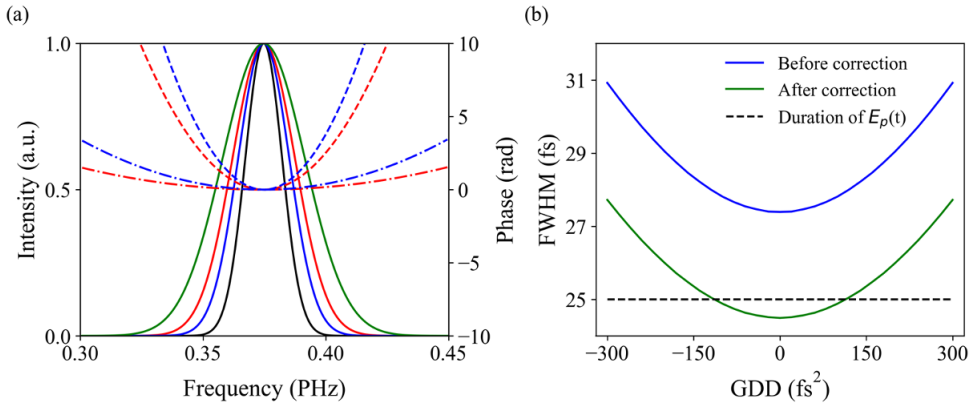

Figure 1. (a) Spectra (solid lines) and spectral phases (dash-dot lines) of $E_{\mathrm{f}}^{5}(t)$ with different dispersions: GDD = 200 fs^2 (red) and GDD = 300 fs^2 (blue). For comparison, the spectral phases (dash lines) of $E_{\mathrm{f}}(t)$ were also plotted for GDD = 200 fs^2 (red) and 300 fs^2 (blue). The black and green solid lines correspond to the spectra of $E_{\mathrm{f}}(t)$ and $E_{\mathrm{f}}^{5}(t)$ without chirp. (b) Measured pulse duration before (blue) and after (green) correction of spectrum for different GDD.

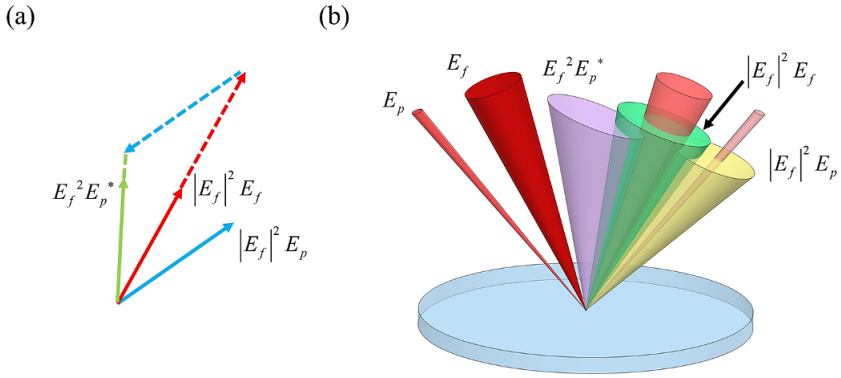

Figure 2. (a) Wave-vectors of the first three terms of Equation (5). (b) RFWM with perturbation on the surface of a solid plate. The red and light red beams represent the fundamental pulse and perturbation pulse, respectively. The three beams generated by four-wave mixing have larger divergence angles, which are green, yellow and purple corresponding to the first three terms on the right-hand side of Equation (5). The incident angle between fundamental and perturbation pulses is exaggerated for clarity.

third-order nonlinear processes are highly intensity dependent, the beam spots of the four-wave mixing are much smaller than $E_{\mathrm{f}}(t)$ and $E_{\mathrm{p}}(t)$ on the surface. Thus, they are more divergent, as shown by the cones in Figure 2(b).

3. Experimental setup and analysis of the results

The experimental setup is shown in Figure 3. The ultrashort pulse is split into two pulses by mask1, that is, the fundamental pulse and perturbation pulse. The diameters of the two holes in mask1 are 6 and 1 mm, respectively. The distance between the centers of the holes is around 4.5 mm, because the beam profile was close to flat-top. We assumed that the energy ratio between the fundamental pulse and the perturbation pulse is about 36. It is well-known that second-harmonic generation (SHG) can occur when a laser pulse is obliquely incident on the surface of a fused silica plate[23]. In our experiment, to eliminate the influence of surface SHG, two pulses were focused and overlapped on the front surface of a thin fused silica plate (100 μm thick) near-normal incidence using a concave mirror with a focal length of 200 mm. Under these conditions, no SHG was detected. The peak intensity of the perturbation pulse is about 0.077% of the fundamental pulse. A lens is used for imaging the RFWM signal to a detector for collecting the RFWM signal, which can be a photodiode, a camera or a spectrometer. In this work, spectrometers were used in the following experiments.

Before the lens, a second mask (mask2) is employed to block $E_{\mathrm{f}}(t)$ and $E_{\mathrm{p}}(t)$. The delay between the fundamental pulse and the perturbation pulse was tuned with a D-shaped mirror mounted on a piezo-linear stage (Physik Instrumente P-621.1) with a step size of 20 nm. The scanning range was set to 100 μm.

Firstly, we measured the ultrashort pulse with center wavelength of 800 nm delivered from a Ti:sapphire laser. The pulse energy before mask1 was approximately 7.6 μJ. The RFWM signal with different delay was measured by a spectrometer (Ocean Insight Maya2000pro) and is shown in Figure 4(a). It is obvious that the fringes emerge only when the two pulses are overlapped temporally. Then we integrate

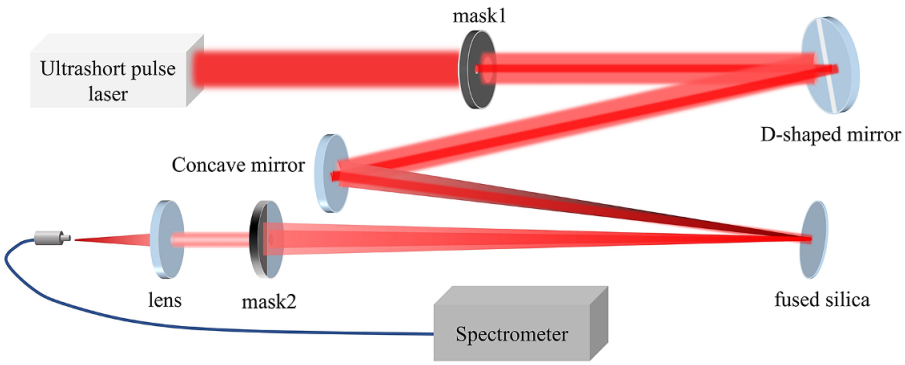

Figure 3. Schematic of the experimental setup. Mask1 is used to split the input pulse into the fundamental pulse and the perturbation pulse. The two pulses are focused by a concave mirror onto the fused silica surface to generate the RFWM signal. The angle between the fundamental and perturbation pulses is exaggerated for clarity. The relative delay between the two pulses is controlled by the D-shape mirror. The RFWM signal is coupled into the detector by a lens after passing through mask2.

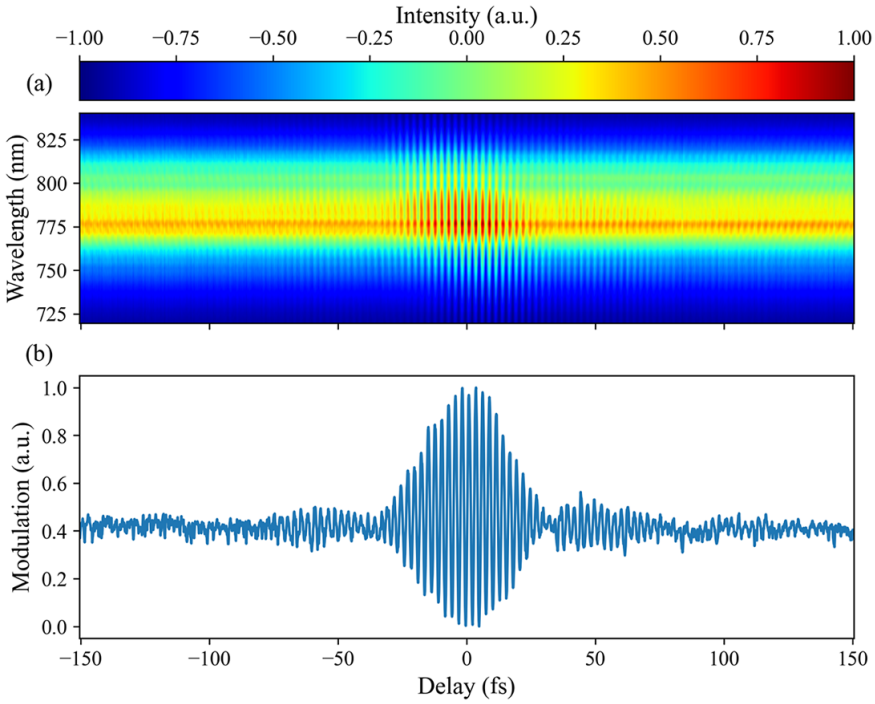

Figure 4. (a) Evolution of the RFWM signal measured by a spectrometer with different relative delays between the fundamental and perturbation pulses. (b) Modulation signal of the RFWM obtained by integrating (a) along the wavelength axis.

and normalize the RFWM signal along the wavelength dimension to obtain the modulation signal of the RFWM, as shown in Figure 4(b).

The noise in Figure 4(b), which is visible before –100 fs and after 100 fs, results from the fluctuation of pulse energy and beam pointing. It can be removed by filtering in the frequency domain. By employing a rectangular window ranging from 700 to 900 nm, the noise can be effectively suppressed (see Figures 5(a), 5(c) and 5(e)). In the following work, we have employed the same method to remove such noise. As shown in Figure 5(a), the measured result shows that the pulse duration is approximately 27 fs. The spectrum and spectral phase of the ultrashort pulse were obtained after the Fourier transform of the waveform, as shown in Figure 5(b). To verify the reliability of this technique, the retrieved spectrum and spectral phase are compared to that obtained with TG-FROG. The results of RFWM sampling agree well with the TG-FROG measurement. To further verify the reliability of the method, we introduced dispersion to the pulses by inserting or removing a piece of 1.3-mm-thick SF11 plate in the perturbation beam path. The measured results through RFWM sampling of positively chirped and negatively chirped pulses are shown in Figures 5(c) and 5(e), respectively. The spectra and spectral phases can be seen in Figures 5(d) and 5(f). The chirped pulses were also characterized by TG-FROG and it confirms the reliability of the RFWM-sampling technique for measuring near-infrared ultrashort pulses (see Figures 5(d) and 5(f)). In addition, the spectra

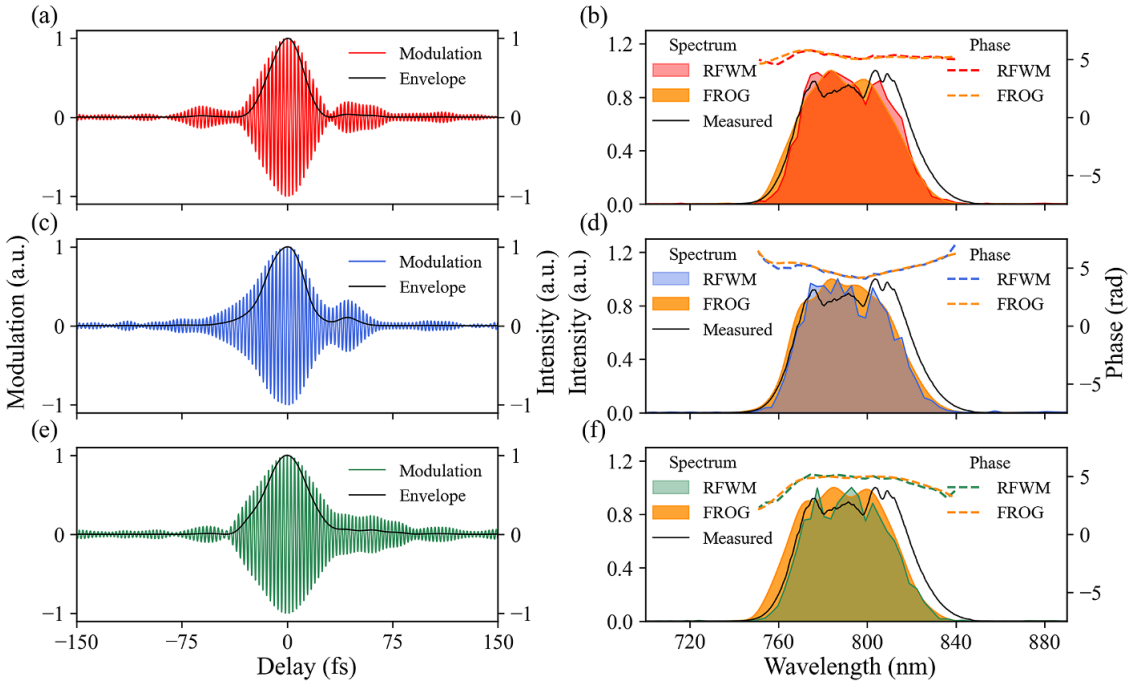

Figure 5. Temporal sampling of 800 nm pulses by RFWM with perturbation. (a), (c), (e) Measured RFWM modulation signal and the envelope of chirp-free, positively chirped and negatively chirped pulses, respectively. (b), (d), (f) Comparison of the spectra and spectral phases retrieved by this method and TG-FROG. The black solid lines illustrate the spectra measured by the spectrometer.

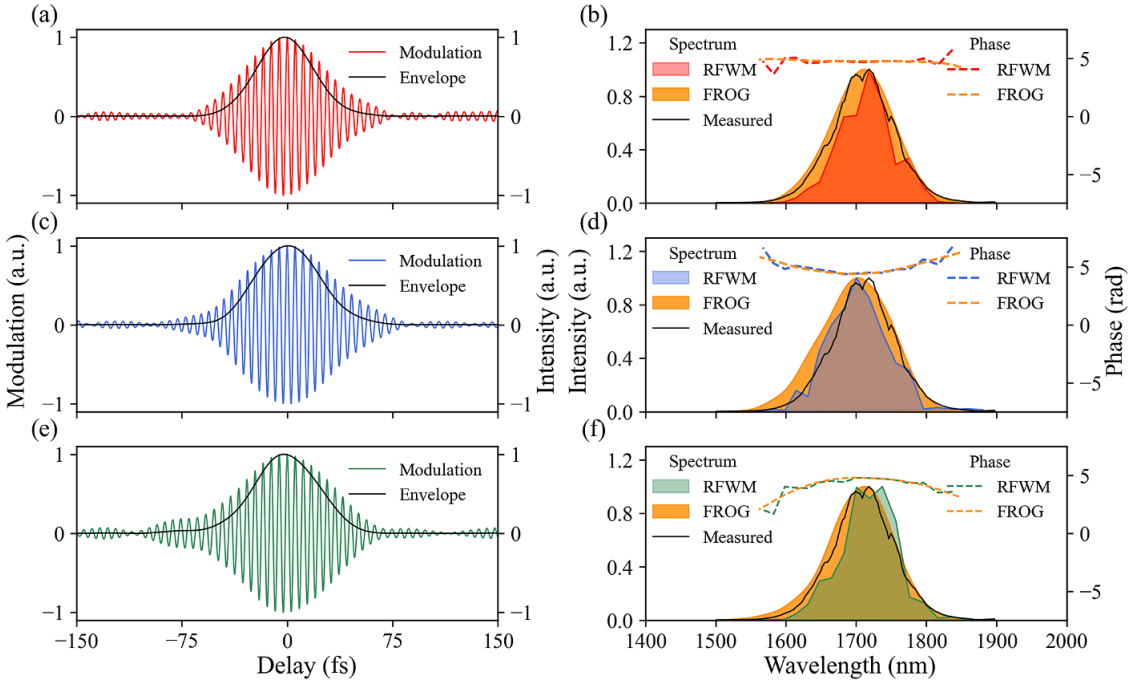

Figure 6. Temporal sampling of pulses at 1700 nm by RFWM with perturbation. (a), (c), (e) Measured RFWM modulation signal and the envelope of chirp-free, positively chirped and negatively chirped pulses, respectively. (b), (d), (f) Comparison of the spectra and spectral phases retrieved by the RFWM with perturbation method and SHG-FROG. The black solid lines illustrate the spectra measured by the spectrometer.

measured with the spectrometer (solid black line in Figures 5(b), 5(d) and 5(f)) are presented for reference as well.

Afterwards, the RFWM-sampling technique was also applied to pulses generated by a TOPAS instrument from Light Conversion with the center wavelength of 1700 nm. After filtering in the frequency domain, the modulation signal is as shown in Figure 6(a), and the pulse duration is approximately 48 fs. We measured the chirped pulses with the RFWM-sampling method and the RFWM modulation signal, and the envelopes are as shown in Figures 6(c)

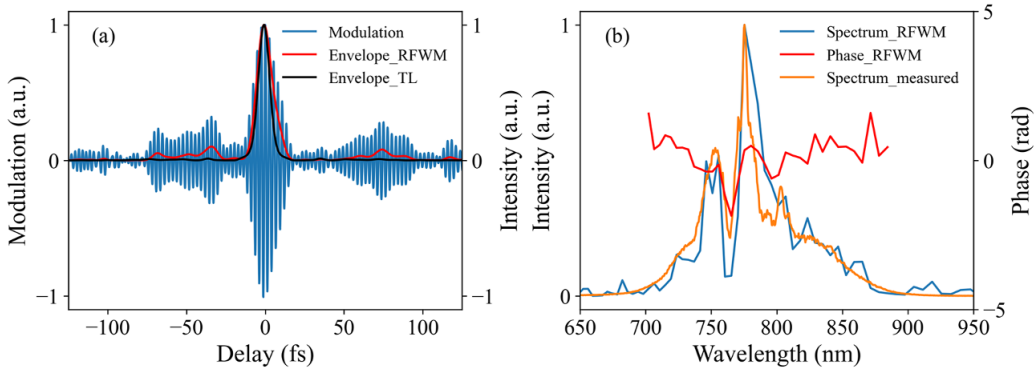

Figure 7. Measurement results of the 800 nm few-cycle pulse by RFWM with perturbation. (a) Modulation signal (blue solid line) and envelope (red solid line) of the few-cycle pulse. The envelope of the TL pulse is shown by the black solid line. (b) Retrieved spectrum (blue solid line) and spectral phase (red solid line). The orange solid line illustrates the spectrum measured by the spectrometer.

and 6(e). The positive chirp and negative chirp were introduced by inserting and removing a piece of 1-mm-thick ZnSe plate in the perturbation beam path, respectively. After Fourier transform of the modulation signal, the spectra and spectral phases are retrieved and are presented in Figures 6(d) and 6(f) accordingly. The spectra and spectral phases were also measured by SHG-FROG. Meanwhile, the spectra were independently measured by the spectrometer as shown with solid black lines in Figures 6(b), 6(d) and 6(f). The retrieved spectra by RFWM sampling are consistent with the spectra obtained by SHG-FROG and the spectrometer. The retrieved phases by RFWM sampling are almost identical to the phases obtained by SHG-FROG.

Finally, we employed the RFWM-sampling method to measure even shorter pulses of few optical cycles, which were obtained by the multiple-thin-plate compression technique to further compress the output pulse from a Ti:sapphire laser. The measured pulse is shown in Figure 7(a). The pulse duration was around 12 fs (full width at half maximum (FWHM)), which was longer than its TL duration of approximately 9 fs (FWHM), as shown by the black solid line in Figure 7(a). The retrieved spectrum (blue solid line) and spectral phase (red solid line) are illustrated in Figure 7(b). It is seen that there was residual dispersion as shown by the spectral phase, which was responsible for the expansion of the pulse duration. The spectrum was simultaneously measured by the spectrometer (orange solid line), which is consistent with the RFWM-sampling method. Because the RFWM occurs at the air–dielectric interface, the requirement of phase-matching is readily fulfilled[24]. Thus, this method can be used to characterize ultra-broadband pulses.

4. Conclusions

In conclusion, we propose a novel all-optical temporal sampling method for ultrashort pulse measurement. This method utilizes the four-wave mixing process with perturbation on solid surfaces. By capturing the RFWM signal from the surface of a 100 μm thin fused silica plate, we have successfully characterized femtosecond pulses with central wavelengths of 800 and 1700 nm. The reliability of this method was verified by comparing it to the FROG measurement. The use of reflection geometry in our measurement scheme allows for measurement of ultrashort pulses as the phase-matching condition is easily satisfied. As a result, the measurement of a few-cycle pulse at 800 nm was demonstrated as well. It is noted that this technique is not suitable for characterization of pulses with severe spatiotemporal coupling. It is necessary to correct the spatiotemporal coupling, for instance, with spatial filters, before the application of this technique. In this work, only 800 and 1700 nm pulses are measured, but based on the current silicon and InGaAs detectors (Thorlabs DET10D2), this method can measure pulses spanning from 200 to 2600 nm with pulse energy at the microjoule level. Because this method relies on the scanning of the delay between two pulses, stable pulse energy is required to obtain reliable measurement. In addition, as demonstrated in the experiment, the influence of energy fluctuation can be mitigated by filtering in the frequency domain. To characterize pulses with wavelength longer than 2600 nm, the four-wave mixing signal cannot be measured with conventional detectors. Thus, other third-order nonlinear processes, such as THG, can be employed. For instance, to measure a pulse with a wavelength as long as 7800 nm, the wavelength of the THG signal is 2600 nm, which can be covered by InGaAs detectors. We believe this method can serve as a reliable tool for the characterization of ultrashort pulses.

Acknowledgements

This work was supported by the National Key R&D Program of China (No. 2022YFE0111500); the National Natural Science Foundation of China (NSFC) (Nos. 62175256, 12104501, 92050107 and 92250303); the Natural Science Basic Research Program of Shaanxi (No. 2019JCW-03);

the Science and Technology Program of Xi'an (No. 202005YK01); the Young Scientist Basic Research Program of the Chinese Academy of Sciences (No. YSBR-091); the Key Deployment Research Program of XIOPM (No. S19-020-III); the Innovation Team in Shaanxi Province (No. J21-029-III); and the Youth Innovation Promotion Association XIOPM-CAS (No. WCH2021002).

References

1. M. Maiuri, M. Garavelli, and G. Cerullo, Am. Chem. Soc. **142**, 3 (2019).
2. F. Krausz and M. Ivanov, Rev. Mod. Phys. **81**, 163 (2009).
3. M. Ossiander, F. Siegrist, V. Shirvanyan, R. Pazourek, A. Sommer, T. Latka, A. Guggenmos, S. Nagele, J. Feist, J. Burgdörfer, R. Kienberger, and M. Schultze, Nat. Phys. **13**, 280 (2017).
4. J. Li and Y. Liu, Ultrafast Sci. **3**, 0049 (2023).
5. J. C. Travers, T. F. Grigorova, C. Brahms, and F. Belli, Nat. Photonics **13**, 547 (2019).
6. J. Pan, Z. Huang, Y. Chen, Z. Luo, F. Yu, D. Wu, T. Chen, D. Liu, Y. Yu, W. He, X. Jiang, M. Pang, Y. Leng, and R. Li, Laser Photonics Rev. **18**, 2400531 (2024).
7. T. Chen, J. Pan, Z. Huang, Y. Yu, D. Liu, X. Chang, Z. Liu, W. He, X. Jiang, M. Pang, Y. Leng, and R. Li, Nat. Commun. **15**, 8671 (2024).
8. L. Wang, G. Tóth, J. Hebling, and F. Kärtner, Laser Photonics Rev. **14**, 2000021 (2020).
9. Y. E, L. Zhang, A. Tcypkin, S. Kozlov, C. Zhang, and X. Zhang, Ultrafast Sci. **2021**, 9892763 (2021).
10. G. Mourou, Rev. Mod. Phys. **91**, 030501 (2019).
11. J. Götzfried, A. Döpp, M. F. Gilljohann, F. M. Foerster, H. Ding, S. Schindler, G. Schilling, A. Buck, L. Veisz, and S. Karsch, Phys. Rev. X **10**, 041015 (2020).
12. R. Trebino, K. W. DeLong, D. N. Fittinghoff, J. N. Sweetser, M. A. Krumbügel, B. A. Richman, and D. J. Kane, Rev. Sci. Instrum. **68**, 3277 (1997).
13. M. Miranda, T. Fordell, C. Arnold, A. L'Huillier, and H. Crespo, Opt. Express **20**, 688 (2012).
14. J. Itatani, F. Quéré, G. L. Yudin, M. Y. Ivanov, F. Krausz, and P. B. Corkum, Phys. Rev. Lett. **88**, 173903 (2002).
15. K. T. Kim, C. Zhang, A. D. Shiner, B. E. Schmidt, F. Légaré, D. M. Villeneuve, and P. B. Corkum, Nat. Photonics **7**, 958 (2013).
16. D. Zimin, M. Weidman, J. Schötz, M. F. Kling, V. S. Yakovlev, F. Krausz, and N. Karpowicz, Optica **8**, 586 (2021).
17. S. B. Park, K. Kim, W. Cho, S. I. Hwang, I. Ivanov, C. H. Nam, and K. T. Kim, Optica **5**, 402 (2018).
18. W. Cho, S. I. Hwang, C. H. Nam, M. R. Bionta, P. Lassonde, B. E. Schmidt, H. Ibrahim, F. Légaré, and K. T. Kim, Sci. Rep. **9**, 16067 (2019).
19. P. Huang, H. Yuan, H. Cao, H. Wang, X. Wang, Y. Wang, W. Zhao, and Y. Fu, Opt. Lett. **47**, 5369 (2022).
20. P. Huang, H. Yuan, H. Cao, H. Wang, X. Wang, Y. Wang, W. Zhao, and Y. Fu, Opt. Lett. **48**, 2154 (2023).
21. R. W. Boyd, *Nonlinear Optics*, 3rd edition (Academic Press, 2008), p. 12.
22. E. J. Takahashi, Y. Fu, and K. Midorikawa, Opt. Lett. **40**, 4835 (2015).
23. F. J. Rodriguez, F. X. Wang, and M. Kauranen, Opt. Express **16**, 8704 (2008).
24. T. Gomes, M. Canhota, and H. Crespo, Opt. Lett. **47**, 3660 (2022).